Supporting Information of

Chemical Transformation of a Long-Chain Alkyl Organosulfate via Heterogeneous OH Oxidation: A Case Study of Sodium Dodecyl Sulfate

Sze In Madeleine Ng[1], Kwan Hung Ng[2], Pui Wo Felix Yeung[2], Rongshuang Xu[1], Pui-Kin So[3], Yuanlong Huang[4], Jian Zhen Yu[5], Chun Kit K. Choi[6], Ying-Lung Steve Tse[2*], Man Nin Chan[1,7*]

[1]Earth System Science Programme, Faculty of Science, The Chinese University of Hong Kong, Hong Kong, China
[2]Departemnt of Chemistry, The Chinese University of Hong Kong, Hong Kong, China
[3]The University Research Facility in Life Sciences, The Hong Kong Polytechnic University, Hong Kong, China
[4]Division of Geological and Planetary Sciences, California Institute of Technology, Pasadena, California 91125, USA
[5]Department of Chemistry, The Hong Kong University of Science and Technology, Hong Kong, China
[6]Department of Chemical Pathology, The Chinese University of Hong Kong, Hong Kong, China
[7]The Institute of Environment, Energy and Sustainability, The Chinese University of Hong Kong, Hong Kong, China

Corresponding authors:
Ying-Lung Steve Tse: stevetse@cuhk.edu.hk, Man Nin Chan: mnchan@cuhk.edu.hk

Table S1. Oxygenated C_{12}-OS and short-chain OS detected upon heterogeneous OH oxidation of dodecyl OS, and their relevance to ambient samples

Chemical formula $[M–H]^-$	Theoretical mass	Detected mass (mass error)	Field studies characterizing their presence as alkyl OS or derivatives of alkyl OS in atmospheric aerosols
Parent OS: Dodecyl OS			
$C_{12}H_{25}O_4S^-$	265.1479	265.1474 (-1.88 ppm)	Hettiyadura *et al.*[1], Cochran *et al.*[2], Blair *et al.*[3], Wang *et al.*[4], 0.20–0.65 ng m^{-3} (Kanellopoulos *et al.*[5])
Oxygenated C_{12}-OS			
$C_{12}H_{23}O_5S^-$	279.1272	279.1268 (-1.43 ppm)	Kuang *et al.*[6], Blair *et al.*[3], Wang *et al.*[4], 3.14–19.56 ng m^{-3} (Riva *et al.*[7])[a]
$C_{12}H_{25}O_5S^-$	281.1428	281.1422 (-2.13 ppm)	Blair *et al.*[3]
$C_{12}H_{21}O_6S^-$	293.1064	293.1059 (-1.71 ppm)	Kuang *et al.*[6], Blair *et al.*[3]
$C_{12}H_{23}O_6S^-$	295.1221	295.1215 (-2.03 ppm)	Kuang *et al.*[6], Blair *et al.*[3]
$C_{12}H_{25}O_6S^-$	297.1377	297.1370 (-2.36 ppm)	Blair *et al.*[3]
$C_{12}H_{19}O_7S^-$	307.0857	307.0851 (-1.95 ppm)	Kuang *et al.*[6], Blair *et al.*[3]
$C_{12}H_{21}O_7S^-$	309.1013	309.1006 (-2.26 ppm)	Kuang *et al.*[6], Blair *et al.*[3]
$C_{12}H_{23}O_7S^-$	311.1170	311.1163 (-2.25 ppm)	Kuang *et al.*[6], Blair *et al.*[3]
Oxygenated short-chain OS (C_6- to C_{10}-OS) (+ 1 × O)			
$C_6H_{11}O_5S^-$	195.0333	195.0331 (-1.03 ppm)	Kuang *et al.*[6], Blair *et al.*[3]
$C_7H_{13}O_5S^-$	209.0489	209.0485 (-1.91 ppm)	Kuang *et al.*[6], Blair *et al.*[3], Wang *et al.*[4]
$C_8H_{15}O_5S^-$	223.0646	223.0643 (-1.34 ppm)	Kuang *et al.*[6], Blair *et al.*[3]
$C_9H_{17}O_5S^-$	237.0802	237.0798 (-1.68 ppm)	Kuang *et al.*[6], Blair *et al.*[3], Wang *et al.*[4], 9.35–12.40 ng m^{-3} (Riva *et al.*[7])[b]
Oxygenated short-chain OS (C_6- to C_{10}-OS) (+ 2 × O)			
$C_6H_{11}O_6S^-$	211.0282	211.0279 (-1.42 ppm)	Kuang *et al.*[6], Blair *et al.*[3]
$C_7H_{13}O_6S^-$	211.0438	211.0434 (-1.78 ppm)	Kuang *et al.*[6], Blair *et al.*[3]
$C_8H_{15}O_6S^-$	239.0595	239.0591 (-1.67 ppm)	Kuang *et al.*[6], Blair *et al.*[3]
$C_9H_{17}O_6S^-$	253.0751	253.0746 (-1.98 ppm)	Kuang *et al.*[6], Blair *et al.*[3]
$C_{10}H_{19}O_6S^-$	267.0908	267.0904 (-1.50 ppm)	Kuang *et al.*[6], Blair *et al.*[3]

[a] Concentrations in Lahore, Pakistan, quantified using octyl sulfate OS as surrogate ($C_8H_{17}O_4S^-$).[7]

[b] Concentrations in Lahore, Pakistan, quantified using authentic OS as surrogate (3-pinanol-2-hydrogen sulfate; $C_9H_{13}O_6S^-$).[7]

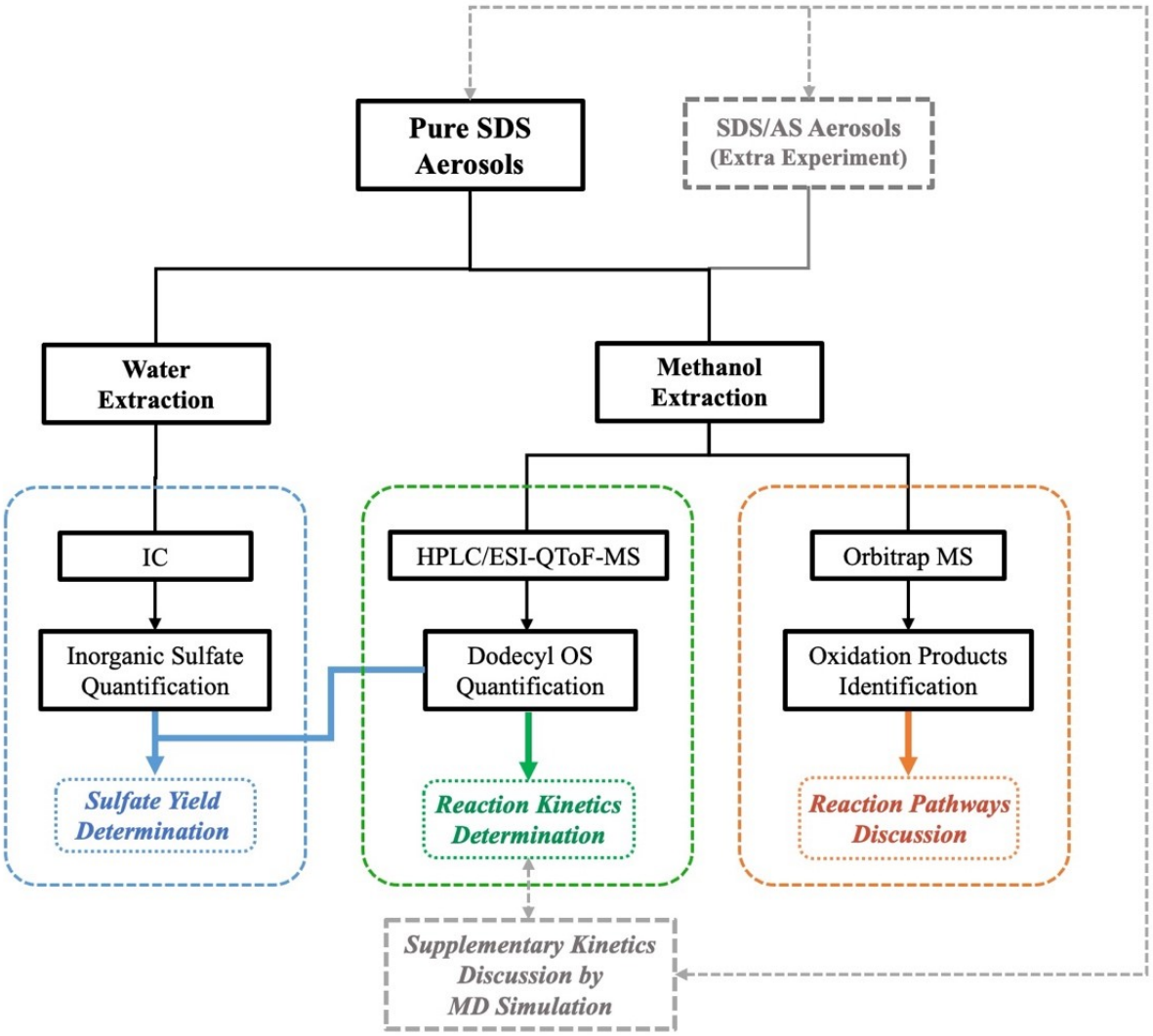

Scheme S1. An overview of chemical analysis for the product identification and reaction kinetic determination performed in this study. Experiments on SDS/AS aerosol were only subjected to chemical kinetics investigation; examination on the effect of AS on products formation was out of the scope in this study.

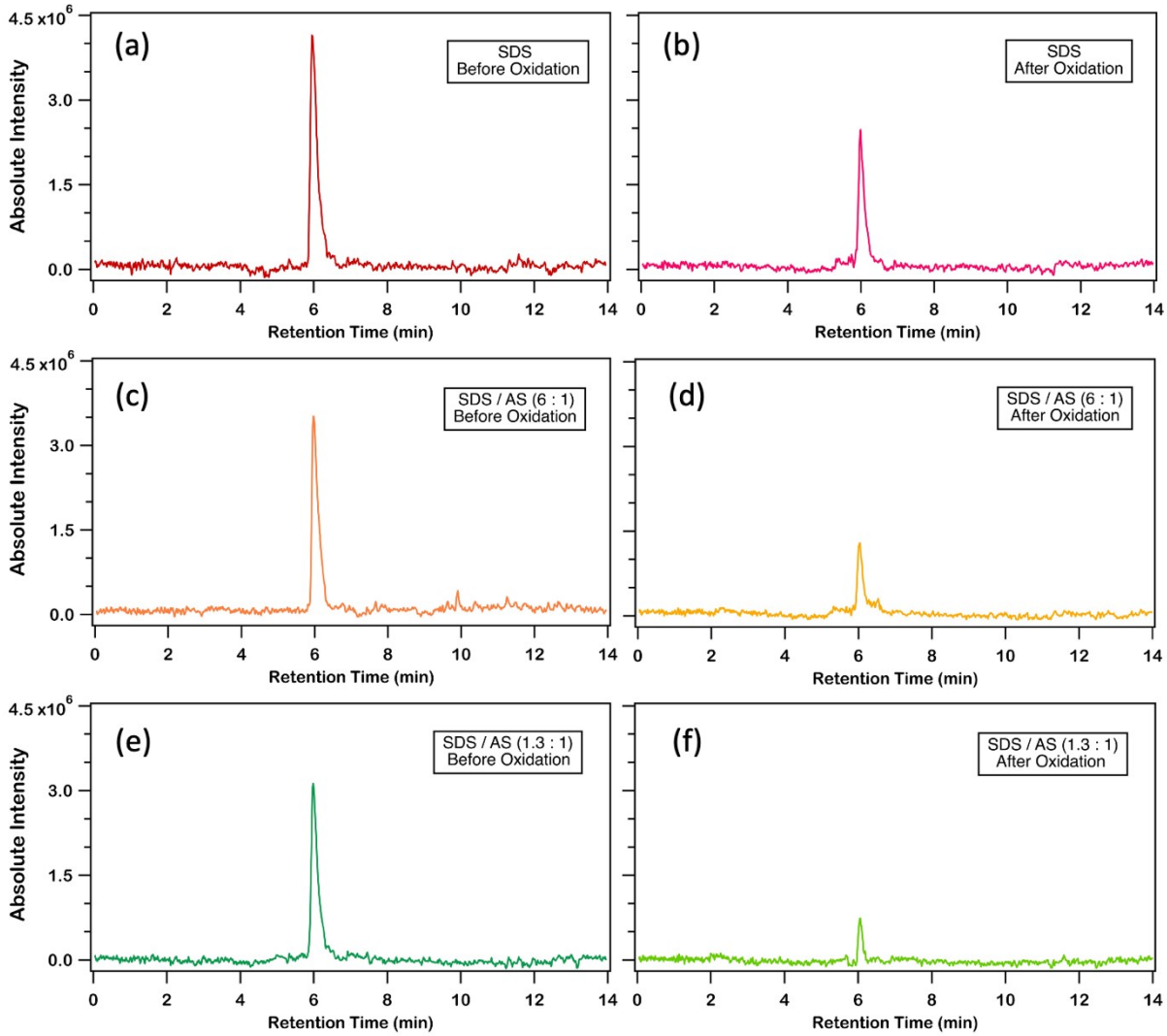

20 **Figure S1**. Total ion chromatogram (TIC) of **(a)** SDS aerosols and **(c-f)** SDS/AS aerosols characterized by the UHPLC/ESI-QToF-MS.

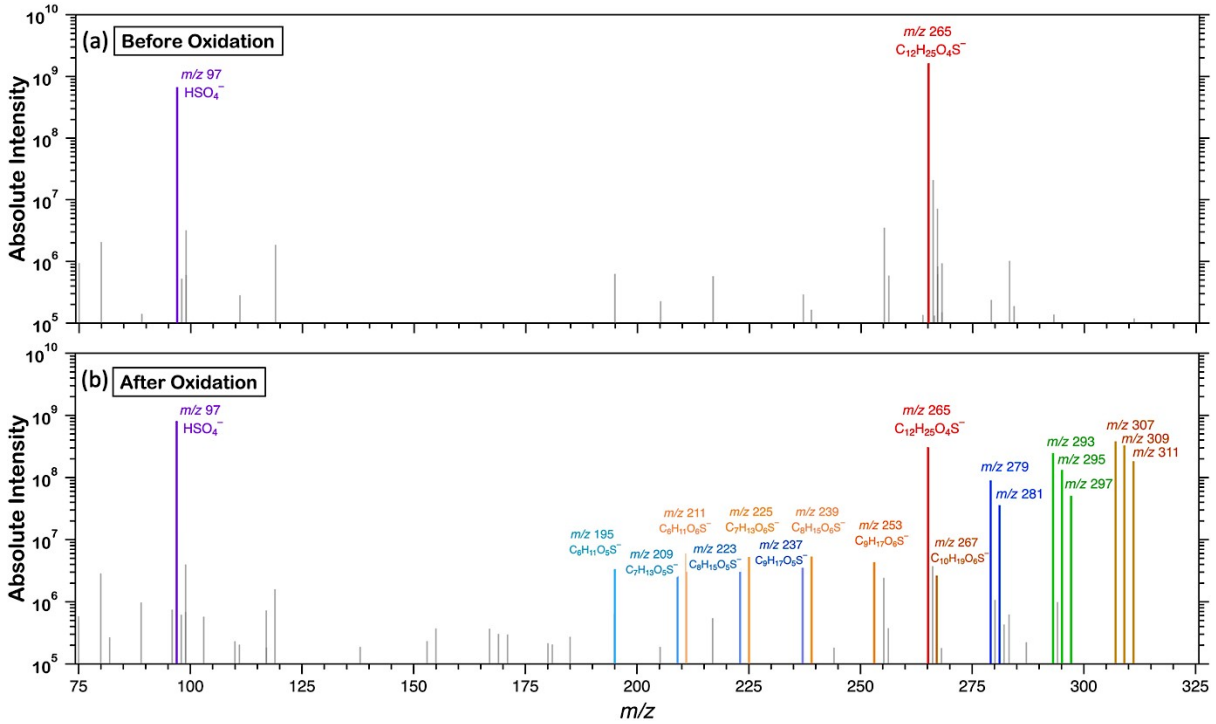

Figure S2. Aerosol mass spectra (y-axis in logarithmic scale) acquired by an ultrahigh-resolution mass spectrometer **(a)** before and **(b)** after heterogeneous OH oxidation of SDS/AS (1.3 : 1) aerosols. The *m/z* of 279 and 281 (1st generation products, in blue) represent $C_{12}H_{23}O_5S^-$ and $C_{12}H_{25}O_5S^-$; *m/z* of 293, 295, and 297 (2nd generation products, in green) represent $C_{12}H_{21}O_6S^-$, $C_{12}H_{23}O_6S^-$, and $C_{12}H_{25}O_6S^-$; *m/z* of 307, 309, and 311 (3rd generation products, in yellowish brown) represent $C_{12}H_{19}O_7S^-$, $C_{12}H_{21}O_7S^-$, and $C_{12}H_{23}O_7S^-$, respectively. The peaks in light grey are background ions.

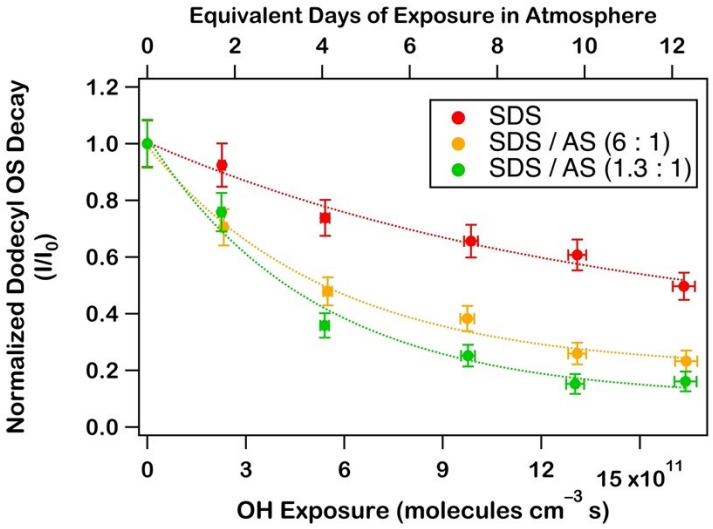

Figure S3. Normalized decay of SDS/AS aerosols containing different mass ratio of SDS and AS upon heterogeneous OH oxidation as a function of OH exposure.

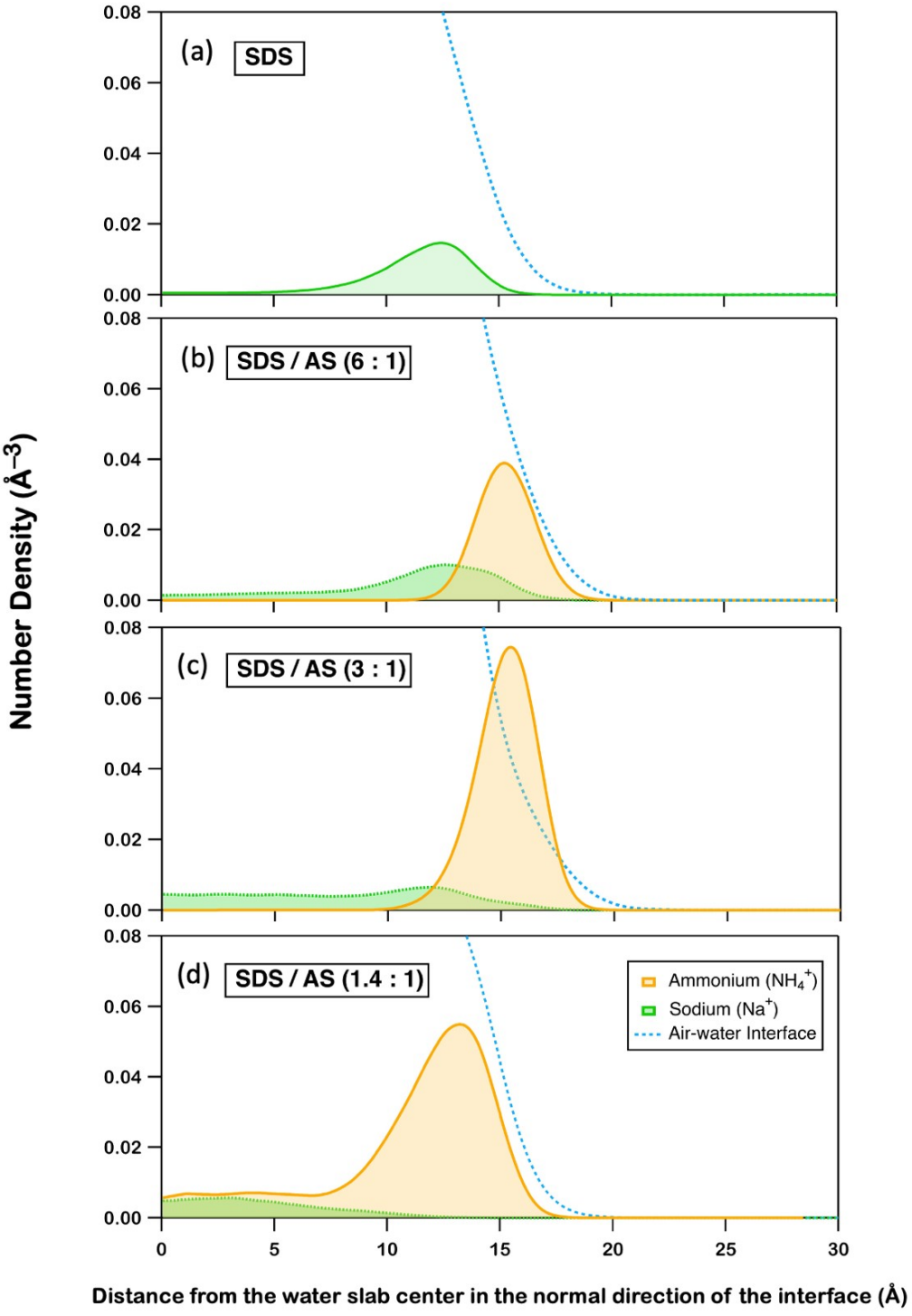

Figure S4. Number density profiles of the cations (Na^+ and NH_4^+) across *z*-distance from the water slab center for different SDS/AS mass ratios **(a-d)**. Displacement of Na^+ by NH_4^+ near the air-water interface is visualized.

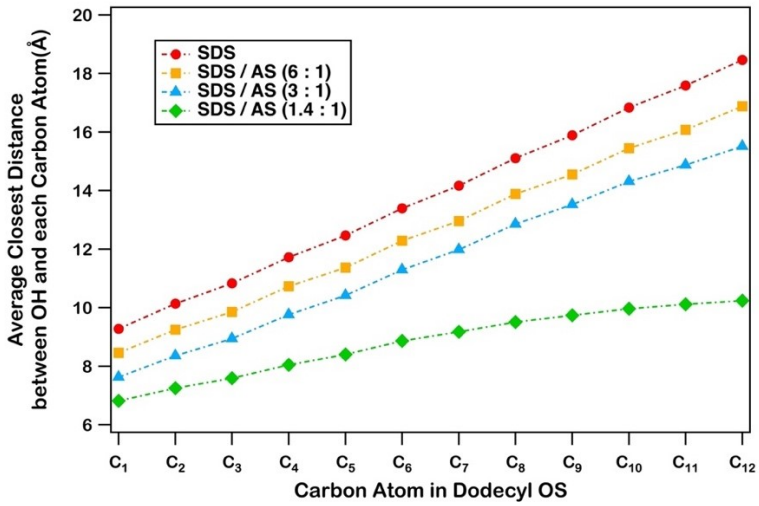

Figure S5. Average closest possible distance between each carbon atom in $C_{12}H_{25}O_4S^-$ and OH for different mass ratios. C_n is the n^{th} carbon atom bonded next to $-OSO_3^-$ group. The average was carried out over multiple OH radicals.

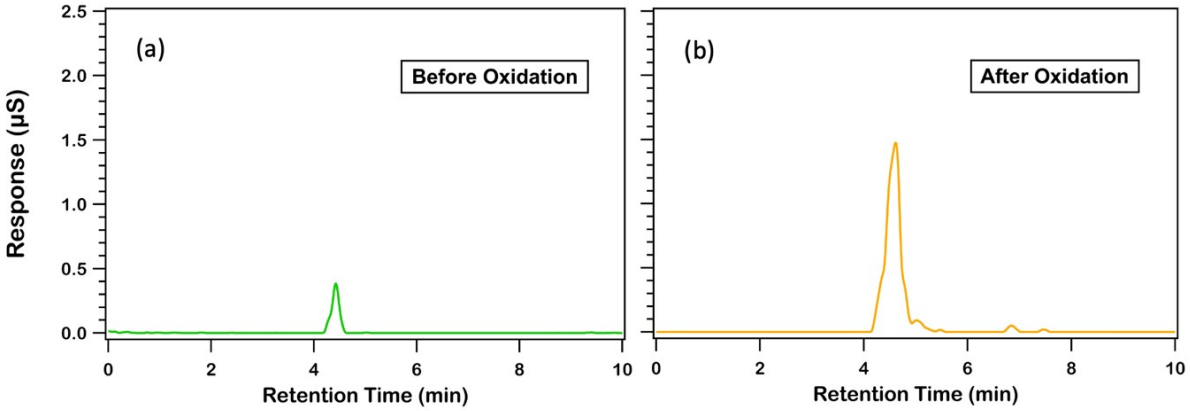

Figure S6. The ion chromatograms **(a)** before and **(b)** after OH oxidation of SDS aerosols. Total quantity of sulfate after oxidation was determined to be small.

Section S1. Chemical Analysis

Scheme S1 depicts the overview of the chemical analysis for product identification and reaction kinetic determination. First, filters were extracted twice with 5 mL methanol in an ultrasonic bath each for an hour. Extracts were then filtered through a 0.2 μm polytetrafluoroethylene (PTFE) syringe filter and combined. 200 μL of the extract was blown to dryness under a gentle stream of ultrapure N_2 at room temperature and then reconstituted in 1 mL methanol–water (1:1 vol/vol). The reconstituted extracts were subjected to chemical analysis for the detection of reaction products and the quantification of dodecyl OS. We selected methanol for extraction since it is a standard solvent for mass spectrometry analysis. We acknowledge that some organic compounds such as carbonyls and carboxylic acids would possibly react with methanol to form esters, hemiacetals, and acetals during extraction or electrospray ionization.[8] We have taken this effect into consideration during product analysis, by confirming that the detected intensities of these potential products are negligible when compared to their precursors. In addition to methanol extraction, a set of duplicated filters were extracted in 5 mL double-deionized water (18.2 MΩ cm) in an ultrasonic bath for an hour. These extracts were analyzed by ion chromatography (IC) for quantification of inorganic sulfates.

Product Identification

To identify the functionalized and fragmented products of dodecyl OS during heterogeneous OH oxidation, 100 μL of each reconstituted methanol-extract was directly injected using a gas-tight Hamilton syringe into an ultra-high-resolution mass spectrometer (Thermo Scientific, Orbitrap Eclipse Tribrid), utilizing electrospray ionization (ESI) source and Orbitrap mass analyzer operating in negative ion mode. The injection flow rate was 25 μL min^{-1}. The ESI source was operated at negative ion mode with spray voltage of 3 kV and 325 °C for sheath gas temperature. Since OS are ionic compounds, negative ions of SDS ($C_{12}H_{25}O_4S^-$), its functionalized products and fragmented products can be detected effectively.[1, 9, 10] Mass spectra were collected with m/z = 50–1000 at a resolution of about 500,000 FWHM and analyzed using Xcalibur software. The top 50 ions of the highest intensities with signal-to-noise ratio ≥ 10 were exported. In the Xcalibur software, a maximum of 20 ^{12}C atoms, 50 ^{1}H atoms, 20 ^{16}O atoms, and 2 ^{32}S atoms were allowed in mathematical deduction of molecular formulas of the detected ions. The ions with deduced formula of $C_cH_hO_{o+4}S^-$ were OS. Deviation between the theoretical mass and detected mass of each derived chemical species did not exceed ± 3.0 ppm.

Dodecyl OS Quantification

To quantify the amount of dodecyl OS at each OH exposure, the reconstituted extracts were injected into an Agilent 1290 UHPLC5 system equipped with an ESI source, interfaced to an Agilent 6540 Quadrupole-Time-of-Flight Mass Spectrometer (UHPLC/ESI-QToF-MS). 5 μL of each reconstituted extract was injected and separated by an Acquity UPLC HSS T3 column (2.1 mm × 100 mm, 1.8 μm; Waters, Milford, MA) with mobile phase consisting of water (H_2O, eluent A) and methanol (eluent B), each containing 0.1 % formic acid. The flow rate was set at 0.3 mL min^{-1}. Gradient elution program was optimized as follows: eluent B was initially set at 30 % for the first 2.0 min, and was gradually boosted to reach 95 % at 10.0 min; then was decreased to 30 % within 0.1 min, and held for 3.9 min. The ESI source was operated at negative ion mode with 2.8 kV for capillary voltage, 120 V for fragment, 320 °C for sheath gas temperature, 8 L min^{-1} for drying gas flow, and 45 psi for nebulizer pressure. Mass spectra were acquired across the range m/z 50–700 at 4 GHz, at a resolution of 40,000 FWHM. Data were analyzed using Mass Hunter Qualitative software (version B.07.00 Agilent Technologies).

The total amount of dodecyl OS at a given OH exposure was proportional to its peak area in the chromatogram, and was determined using an external SDS standard calibration curve ($R^2 = 0.99$). The extraction efficiency was determined to be 87.9 ± 1.7 % by measuring the recovery of dodecyl OS standard spiked onto blank filters following the same experimental protocol. It further indicated that methanol could be considered an effective solvent for extracting dodecyl OS collected on filters. The uncertainty for the measurement of SDS is determined and discussed in the **Section S2**. The SDS concentrations have been corrected for the extraction efficiency.

Inorganic Sulfate Quantification

The amount of inorganic sulfate formed upon oxidation was quantified using IC method. Operating conditions have been given by Huang *et al*.[11] Briefly, the water-extracts were filtered by PTFE and injected into an ion chromatograph (Dionex ICS-1100). AS11-HC analytical column (IonPac, 4 × 250 mm) and AG11-HC guard column (IonPac, 4 × 50 mm) with 15 mmol L^{-1} NaOH eluent were employed for effective separation of anions.

Justified by our previous study, both retention time and response of sodium sulfate (Na_2SO_4) standard in IC chromatogram was identical to that of the sodium bisulfate ($NaHSO_4$) standard.[12] As HSO_4^- is converted to SO_4^{2-} upon mixing with NaOH, the total amount of inorganic sulfate quantified was represented by that of SO_4^{2-}. Furthermore, the responses of the $NaHSO_4$ and Na_2SO_4 standards are about the same. These would justify the use of the Na_2SO_4 standard for the quantification of HSO_4^- and SO_4^{2-}. The total amount of HSO_4^- and SO_4^{2-} produced upon oxidation at a given OH exposure was proportional to its peak area in the chromatogram, and was determined using an external Na_2SO_4 standard calibration curve. The extraction efficiency was determined to be 90.3 ± 1.5 % by measuring the recovery of the Na_2SO_4 standard spiked onto blank filters.[12] The uncertainty for the measurement of SO_4^{2-} has been discussed in the **Section S2**. The inorganic sulfate concentrations have been corrected for the extraction efficiency.

Section S2. Determination of Measurement Uncertainties

Uncertainty for quantification of dodecyl OS ($C_{12}H_{25}O_4S^-$) and sulfate (SO_4^{2-}) ions

Measurement precisions for the concentration of species *i* (σ_{Ci}) are propagated from precisions of volumetric measurements, chemical composition measurements, blank sample variability and sample repeatability, referring to Bevington *et al.*[13] and Ellison *et al.*[14]. For simplicity, the following equations are used to calculate the uncertainty associated with our filter-based measurements:

$$C_i = \frac{M_i - B_i}{V} \quad (1)$$

$$B_i = \frac{1}{n}\sum_{j=1}^{n} B_{ij} \; for \; B_i > \sigma_{B_i} \quad (2)$$

$$B_i = 0 \; for \; B_i \leq \sigma_{B_i} \quad (3)$$

$$\sigma_{B_i} = STD_{B_i} = [\frac{1}{n-1}\sum_{j=1}^{n}(B_{ij} - B_i)^2]^{\frac{1}{2}} \; for \; STD_{B_i} > SIG_{B_i} \quad (4)$$

$$\sigma_{B_i} = STD_{B_i} = [\frac{1}{n}\sum_{j=1}^{n}(\sigma_{B_{ij}})^2]^{\frac{1}{2}} \; for \; STD_{B_i} \leq SIG_{B_i} \quad (5)$$

$$\frac{\sigma_V}{V} = 0.05 \quad (6)$$

$$\sigma_{C_i} = [\frac{{\sigma_{M_i}}^2 + {\sigma_{B_i}}^2}{V^2} + \frac{{\sigma_V}^2(M_i - B_i)^2}{V^4}]^{\frac{1}{2}} \quad (7)$$

where

B_i = average amount of species *i* on blank samples
B_{ij} = amount of species *i* found on blank sample *j*
C_i = concentration of species *i*
M_i = amount of species *i* on the substrate
n = total number of samples in the sum
SIG_{Bi} = root mean square error (RMSE), the square root of the averaged sum of the squared σ_{Bij}
STD_{Bi} = standard deviation of the blank samples
σ_{Bi} = blank precision of species *i*
σ_{Bij} = precision of species *i* detected on blank sample *j*
σ_{Ci} = propagated precision of concentration of species *i*
σ_{Mi} = precision of amount of species *i* on the substrate
σ_V = precision of sample volume
V = sample volume

The precisions (σ_{Mi}) were determined from duplicate analysis of samples. When duplicate sample analysis is made, the range of results, *R*, is nearly as efficient as the standard deviation since two measures differ by a constant ($1.128\sigma_{Mi} = R$). Based on the blank samples and duplicate samples, coefficients needed for determining uncertainty are given in following table:

Species	Quantification	No. of	No. of	Blank	Duplicate

	method	Blanks	duplicate standard	Precision (σ_{Bi}, mg)	Precision (σ_{Mi}, mg)
Dodecyl OS	UHPLC/ESI-QToF-MS	3	6	0.000	0.0049
Sulfate/ bisulfate	IC	3	3	0.0019	0.0017

Uncertainty for yield of *j*, σ_{yield_j}

$$\sigma_{yield_j} = \left[\frac{\sigma_{Dodecyl\ OS_j}{}^2 + \sigma_{Dodecyl\ OS_0}{}^2}{\left(Dodecyl\ OS_0 - Dodecyl\ OS_j\right)^2} + \frac{\sigma_{sulfate_j}{}^2 + \sigma_{sulfate_0}{}^2}{\left(sulfate_j - sulfate_0\right)^2}\right]^{\frac{1}{2}} \times yield_j$$

where

σ_{yield_j}= precision of molar yield on sample *j*

$\sigma_{Dodecyl\ OS_j}$= precision of dodecyl OS on sample *j*

$\sigma_{Dodecyl\ OS_0}$= precision of dodecyl OS on initial sample (before oxidation)

$\sigma_{sulfate_j}$= precision of sulfate on sample *j*

$\sigma_{sulfate_0}$= precision of sulfate on initial sample (before oxidation)

$Dodecyl\ OS_j$= the amount of dodecyl OS on sample *j*

$Dodecyl\ OS_0$= the amount of dodecyl OS detected on initial sample (before oxidation)

$yield_j$= molar yield for sample *j*

The uncertainty for OH exposure, σ_{exp}

$$\sigma_{exp} = 0.005\ \times OH\ exposure \times \sqrt{\left(16 + \frac{2}{\left(OH\ exposure \times k_{SO_2}\right)^2}\right)}$$

where 0.005 is the precision of SO_2 analyzer (0.5 % of the reading), $k_{SO_2}$is the second-order rate constant of the gas-phase OH and SO_2 reaction: 9×10^{-13}, $cm^3\ molecule^{-1}\ s^{-1}$.

The uncertainty for parent decay index, $\sigma_{\frac{I}{I_0}}$

$$\sigma_{\frac{I}{I_0}} = \frac{I}{I_0} \times \sqrt{\left(\frac{\sigma_I}{I}\right)^2 + \left(\frac{\sigma_{I_0}}{I_0}\right)^2}$$

where I is the concentration of dodecyl OS at a given OH exposure, I_0 is the concentration of dodecyl OS before oxidation, σ_I is the uncertainty of dodecyl OS on sample at a given OH exposure.

The uncertainty for atmospheric lifetime, σ_τ

$$\sigma_\tau = \tau \sqrt{\left(\frac{\sigma_k}{k}\right)^2}$$

where k is the fitted heterogeneous OH rate constant.

Section S3. Molecular Dynamics (MD) Simulations

The simulations aimed to study the interactions between hydroxyl radical OH and a ternary mixture of sodium dodecyl OS (SDS), ammonium sulfate (AS), and water in a droplet. The effect by AS on the kinetic enhancement of SDS aerosol was of particular interest, for the purpose of understanding the role of AS in altering the rate of heterogeneous OH oxidation of dodecyl OS. To investigate, non-reactive all-atom MD simulations were performed to assist in characterizing the possible interactions between dissolved ions and OH; combined with *ab initio* calculations, detailed spatial distributions of OH in different chemical situation can be calculated. The MD simulations of droplets consisting of varying amounts of the mixture components were performed in OPENMM 7.[15] This section is divided into 3 parts:

1. Simulation setups
2. Adjustment of Force Field Parameters
3. Equilibrium Simulation Details

S3.1. Simulation setups

To investigate the role of AS in the reaction between dodecyl sulfate and OH, all of the carbon sites in a dodecyl sulfate molecule were analyzed in terms of the distances between the two reactants. **Figure S7** displays the molecular structure of SDS. The carbon atoms in dodecyl OS are labelled such that C_n is the *n*-th carbon from the sulfate ($–OSO_3^-$) group.

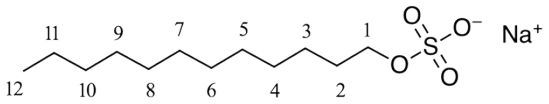

Figure S7. Structure of SDS with labelled carbon numbers.

Electronic polarizability is known to be important in describing ionic interactions in the presence of the air water interface. The electronic polarizability (α) of each nucleus was computed by modeled by Drude oscillators.[16] The charge of a Drude Oscillator q_D is determined by

$$\alpha = \frac{{q_D}^2}{k_D}$$

where k_D was set to 1000 kcal/mol. The SWM4-NDP polarizable water model was used in the simulations.[17] Dodecyl OS ($C_{12}H_{25}SO_4^-$), ammonium (NH_4^+), and sulfate (SO_4^{2-}) were parametrized by GAAMP.[18] Parameters of sodium ion (Na^+) were acquired from Yu *et al.*[19], while those of OH were fitted as described in **S3.2** below.

S3.2. Adjustment of force field parameters

S3.2.1. Hydroxyl radical (OH)

Parameters for the O–H bond and the Lennard-Jones (LJ) interaction were obtained from the general AMBER Force Field (GAFF).[20] Atomic polarizability of oxygen was referenced from the experimental value from CCCBDB database.[21] The remaining parameters, being the partial charges of hydrogen (q_H) and oxygen (q_O) in OH, were fitted to match the free energy of solvation (ΔF) of OH across the air-water interface reported by Roeselová *et al.*,[22] which was computed to be -3.0 ± 0.1

kcal/mol. In order to replicate the reference value of ΔF, simulation of the air-water interface system was performed as shown in **Figure S8a**. The partial charges of OH were varied to yield different ΔF by umbrella sampling [23] as illustrated in **Figure S8b**. The optimal partial charges of OH at ± 0.275 were found to reproduce the reference ΔF.

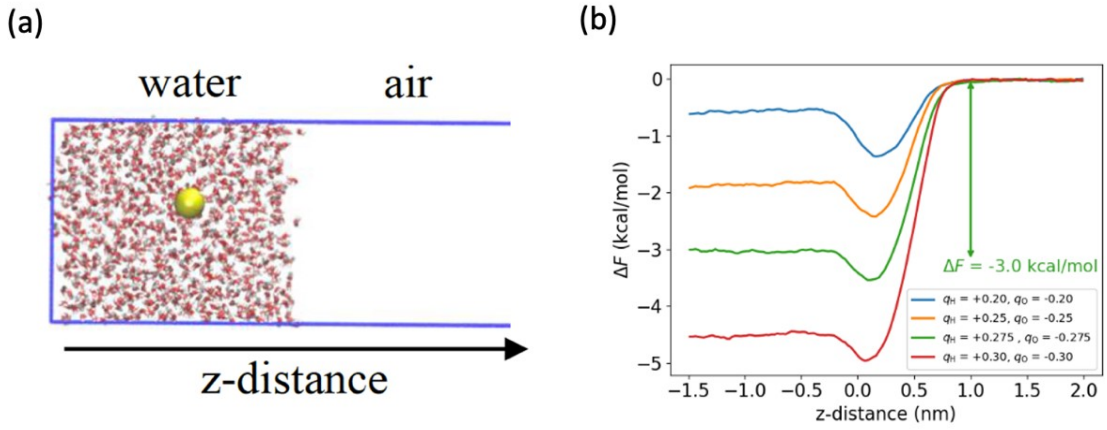

Figure S8. (a) The simulation box of air-water interface, which the yellow sphere represents OH; **(b)** ΔF of OH achieved by umbrella sampling at different q_H and q_O.

S3.2.2. Ammonium sulfate (AS)

Parametrized by GAAMP initially, NH_4^+ and SO_4^{2-} were observed to bound too tightly in our classical MD simulations as shown in the radial distribution function (RDF) between the N atom in NH_4^+ and S atom in SO_4^{2-} in **Figure S9a**. The first peak of the RDF is unusually high and indicates the unphysically over-sticking problem, which should not exist as AS is readily soluble in water. The problem was addressed by adjusting the intermolecular interaction parameters (LJ) between the AS ion pairs to increase the solubility. We adopted the LJ parameters from the work by Lam *et al.*[24] in our AS model generated by GAAMP. The final AS model was able to reproduce the first peak of a reference RDF (**Figure S9b**) in another study by Gopalakrishnan *et al.*[25] and resolve the over-sticking problem.

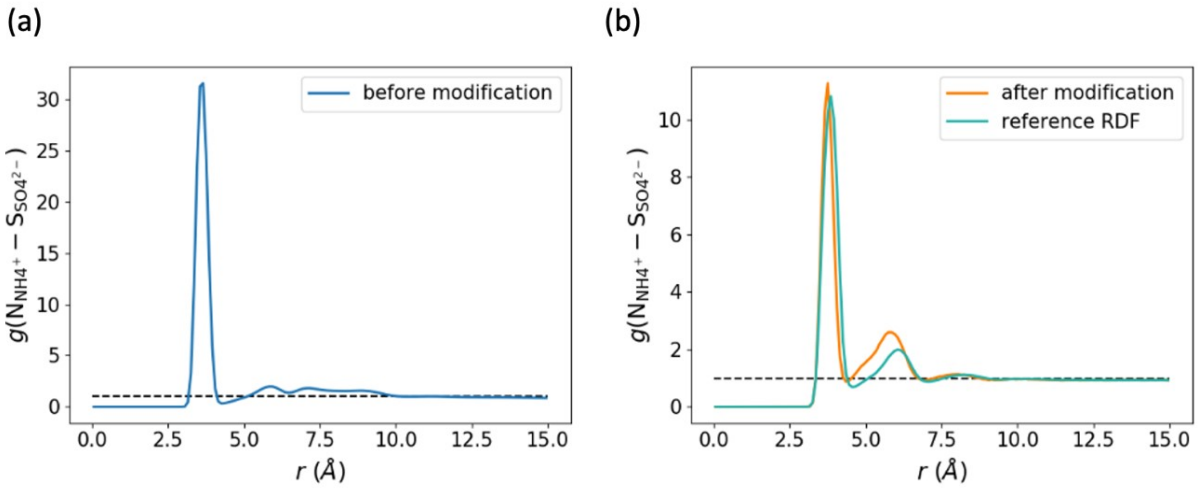

Figure S9. **(a)** RDF between N atom in NH_4^+ and S atom in SO_4^{2-} before modification on the intermolecular interaction parameters (LJ); **(b)** RDF from our modified model and that from the reference model by Gopalakrishnan *et al.*[25] for comparison.

A summary of the partial charges and α is provided in **Figure S10a** and **Figure S10b**, respectively.

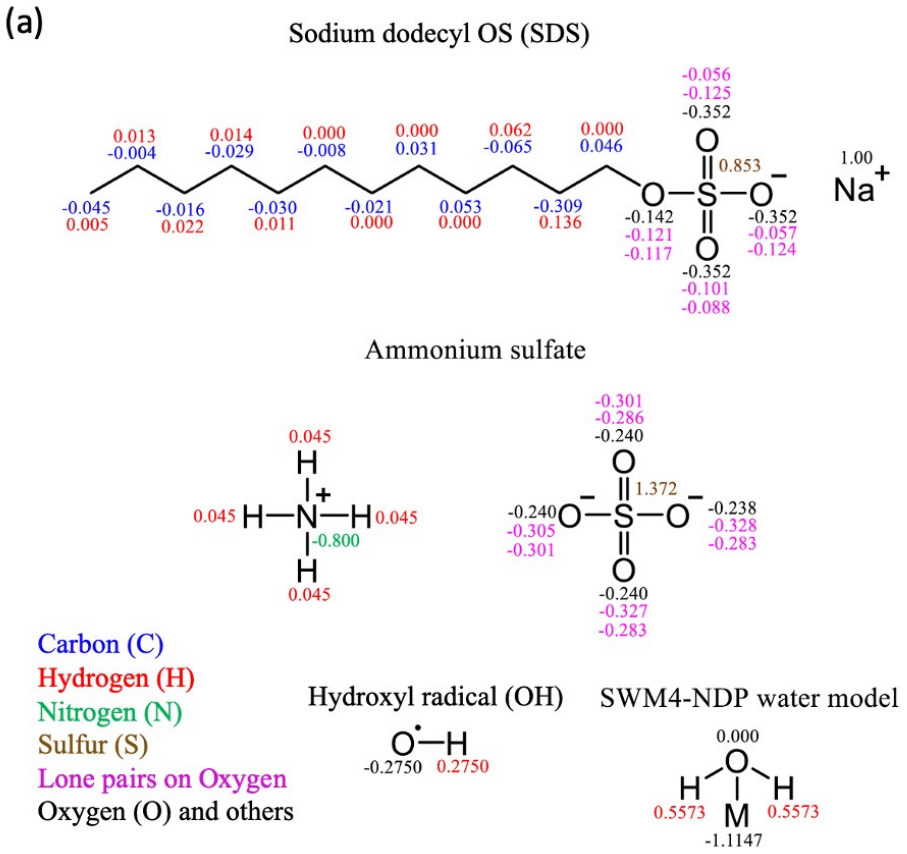

Figure S10. (a) Partial charges and **(b)** polarizability (α) within each molecule.

S3.2.3. Interaction between OH and AS

As there were no reference MD interaction parameters of the two ion–radical pairs (NH_4^+–OH and SO_4^{2-}–OH) available in the literature, we ran *ab initio* quantum mechanical calculations to parameterize the interactions by matching the potential energy surfaces. The *ab initio* MD (AIMD) calculations were performed in CP2K package [26] at the level of calculation of BLYP [27] with D3 dispersion correction,[28] with TZVP basis set and Goedecker-Teter-Hutter (GTH) pseudopotentials.[29] The potential energy (PE) at different configurations at various ion–radical distances *d* (See **Figure S11**) were then evaluated by both our initial classical MD model (before adjustment) and *ab initio* calculations. The comparisons of the PE are **Figure S12a** and **Figure S12b**.

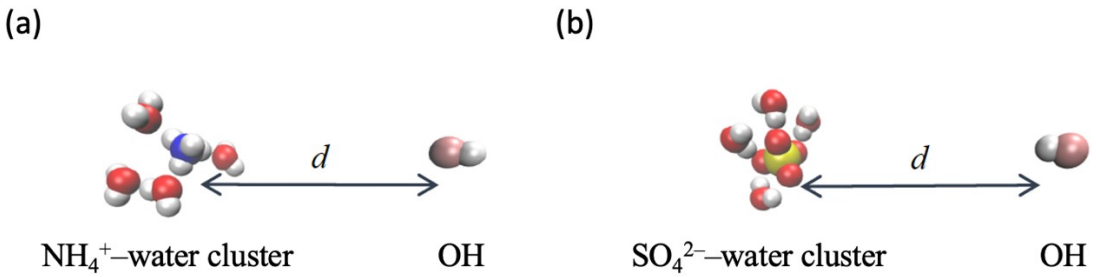

Figure S11. Snapshot of the pair of **(a)** NH_4^+–water cluster and **(b)** SO_4^{2-}–water cluster separated from OH by a distance *d*.

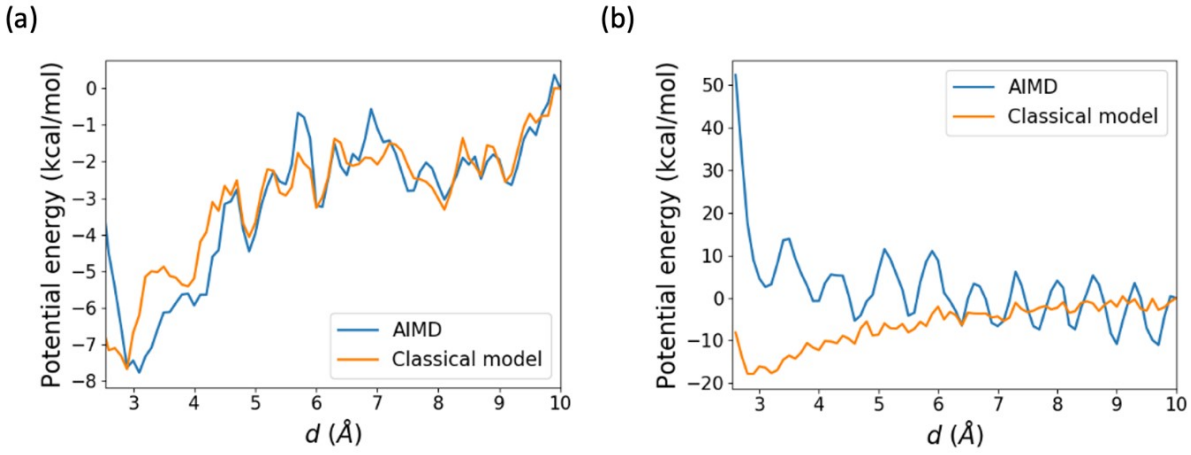

Figure S12. Potential energy (PE) curves calculated from *ab initio* molecular dynamics (AIMD) and from our classical model on: **(a)** NH_4^+–OH, **(b)** SO_4^{2-}–OH pair.

We can see from **Figure S12b** that our initial classical model did not capture the repulsion between SO_4^{2-} and OH in AIMD (i.e. PE increases as the distance decreases). To match the AIMD curve as much as possible, the WCA potential [30] was utilized to replace the LJ potential for the intermolecular interaction between SO_4^{2-} and OH. The WCA potential is essentially a modification of LJ potential by truncation at its potential minimum at $r_0 = 2^{1/6}\sigma$ and an upward shift by ϵ, which is a repulsive potential

as illustrated in **Figure S13a**. The functional form of WCA potential U_{WCA} is described in **Equation S1**.

$$U_{WCA}(r) = \begin{cases} 4\epsilon\left(\left(\frac{\sigma}{r}\right)^{12} - \left(\frac{\sigma}{r}\right)^{6}\right) + \epsilon, & r \le 2^{1/6}\sigma \\ 0, & r > 2^{1/6}\sigma \end{cases} \quad \textbf{(Equation S1)}$$

The WCA potential was adopted between O atom in SO_4^{2-} and O atom in OH. The parameters were optimized that ϵ = 1.5 kcal/mol and σ = 2.68 Å. After replacing the LJ potential by the purely repulsive WCA potential, there is now stronger repulsion between SO_4^{2-} and OH as shown in **Figure S13b** and they no longer stick together.

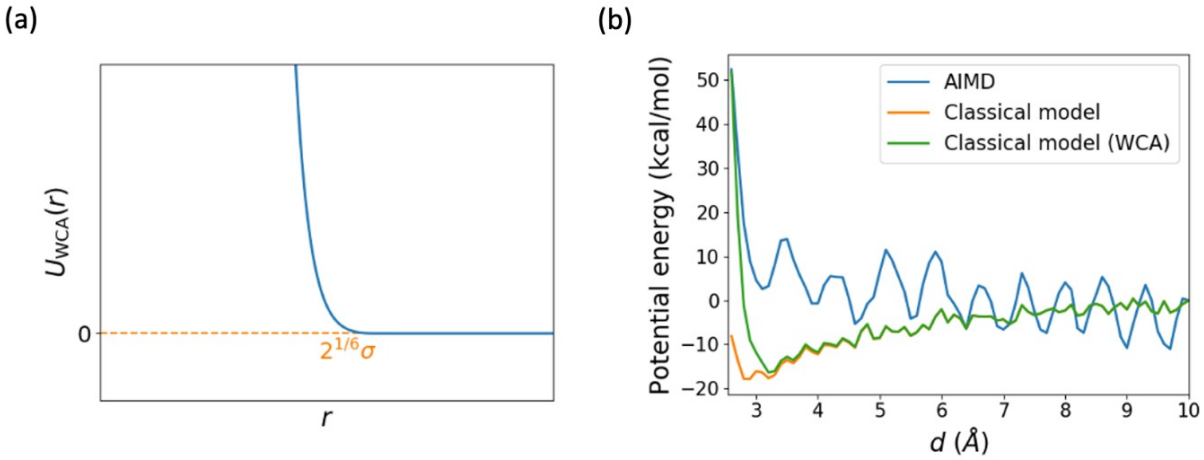

Figure S13. a) WCA potential, which is purely repulsive; b) The PE curves of SO_4^{2-}–OH pair computed using LJ potential in AIMD, WCA potential, and the classical model.

S3.3 Equilibrium simulation details

Simulating a macroscopic atmospheric aerosol with diameter of hundreds of nanometers to a few micrometers by atomistic MD simulation is computationally challenging. Our solution to this size problem was to approximate part of the aerosol as a slab system, illustrated in **Figure S14**. The simulated water slab consisted of OH with dissolved ions from SDS (Na^+, $C_{12}H_{25}O_4S^-$) and AS (NH_4^+, SO_4^{2-}).

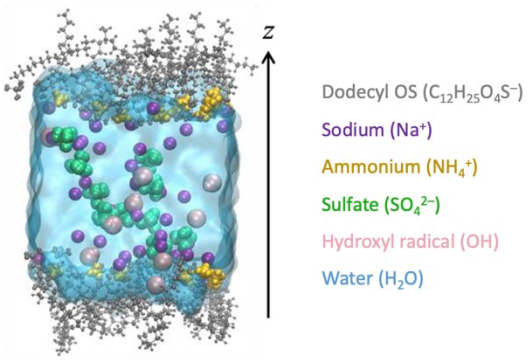

Figure S14. Illustration of a slab system in our MD simulation consisting of all components.

OH radicals were positioned in the water based on our previous observation that most reactions should occur after OH radicals are adsorbed into the aqueous phase and diffuse near OS for reaction.[24, 31] To build the slab system and to qualitatively highlight the role of AS in enhancing the OH reaction kinetic of SDS, different numbers of molecules were studied. The difference in numbers of water molecule in the bulk sought to mimic different mass fractions of aerosol constituents, that may vary due to hygroscopic growth of aerosol under different RH. The changes in SDS–OH distances as a function of AS concentration was assessed to rationalize the ionic effect of dissolved AS on enhancing or suppressing the reaction kinetics. Using the same approach by Faust and Abbatt [32], the mass fractions of water, SDS, and AS in aerosols at 80 % RH and 298 K for different SDS/AS aerosols were estimated by E-AIM II.[33] Based on the modeled mass fractions, simulation slab systems were built (**Table S3**). The mass fractions used in our simulation were as close to those modelled by E-AIM II as possible.

Table S3. Slab systems built in equilibrium MD simulation.

AS : SDS	Mass Fractions of Slab system (mass fractions modelled by E-AIM)		
	Water	SDS	AS
0	0.61	0.39	0
1 : 6	0.58 (0.57)	0.36 (0.37)	0.06 (0.06)
1 : 3	0.55 (0.57)	0.34 (0.33)	0.11 (0.10)
1 : 1.4	0.58 (0.57)	0.24 (0.25)	0.17 (0.18)

The time step of the simulations was 1 femtosecond. During simulation, each system was first equilibrated for 10 ns. Then production data was collected and averaged from 10 independent 5-ns production runs with different equilibrated configurations. Both equilibration and production runs were performed under constant *NVT* dynamics with Langevin thermostat for Drude oscillators. Periodic boundary conditions were applied to all dimensions of the simulation box. Except that the WCA potential had a cut-off of 0.3 nm, all LJ interactions as well as the real space of the particle-mesh Ewald were assigned a cut-off distance of 1.0 nm.

References

1. A. P. S. Hettiyadura, T. Jayarathne, K. Baumann, A. H. Goldstein, J. A. de Gouw, A. Koss, F. N. Keutsch, K. Skog and E. A. Stone, Qualitative and quantitative analysis of atmospheric organosulfates in Centreville, Alabama, *Atmos. Chem. Phys.*, 2017, **17**, 1343-1359.
2. R. E. Cochran, O. Laskina, T. Jayarathne, A. Laskin, J. Laskin, P. Lin, C. Sultana, C. Lee, K. A. Moore, C. D. Cappa, T. H. Bertram, K. A. Prather, V. H. Grassian and E. A. Stone, Analysis of Organic Anionic Surfactants in Fine and Coarse Fractions of Freshly Emitted Sea Spray Aerosol, *Environmental Science & Technology*, 2016, **50**, 2477-2486.
3. S. L. Blair, A. C. MacMillan, G. T. Drozd, A. H. Goldstein, R. K. Chu, L. Paša-Tolić, J. B. Shaw, N. Tolić, P. Lin, J. Laskin, A. Laskin and S. A. Nizkorodov, Molecular Characterization of Organosulfur Compounds in Biodiesel and Diesel Fuel Secondary Organic Aerosol, *Environmental Science & Technology*, 2017, **51**, 119-127.
4. K. Wang, Y. Zhang, R.-J. Huang, M. Wang, H. Ni, C. J. Kampf, Y. Cheng, M. Bilde, M. Glasius and T. Hoffmann, Molecular Characterization and Source Identification of Atmospheric Particulate Organosulfates Using Ultrahigh Resolution Mass Spectrometry, *Environmental Science & Technology*, 2019, **53**, 6192-6202.
5. P. G. Kanellopoulos, S. P. Kotsaki, E. Chrysochou, K. Koukoulakis, N. Zacharopoulos, A. Philippopoulos and E. Bakeas, PM2.5-bound organosulfates in two Eastern Mediterranean cities: The dominance of isoprene organosulfates, *Chemosphere*, 2022, **297**, 134103.
6. B. Y. Kuang, P. Lin, M. Hu and J. Z. Yu, Aerosol size distribution characteristics of organosulfates in the Pearl River Delta region, China, *Atmospheric Environment*, 2016, **130**, 23-35.
7. M. Riva, T. Da Silva Barbosa, Y. H. Lin, E. A. Stone, A. Gold and J. D. Surratt, Chemical characterization of organosulfates in secondary organic aerosol derived from the photooxidation of alkanes, *Atmos. Chem. Phys.*, 2016, **16**, 11001-11018.
8. A. P. Bateman, M. L. Walser, Y. Desyaterik, J. Laskin, A. Laskin and S. A. Nizkorodov, The Effect of Solvent on the Analysis of Secondary Organic Aerosol Using Electrospray Ionization Mass Spectrometry, *Environmental Science & Technology*, 2008, **42**, 7341-7346.
9. P. Lin, J. Z. Yu, G. Engling and M. Kalberer, Organosulfates in Humic-like Substance Fraction Isolated from Aerosols at Seven Locations in East Asia: A Study by Ultra-High-Resolution Mass Spectrometry, *Environmental Science & Technology*, 2012, **46**, 13118-13127.
10. J. D. Surratt, Y. Gómez-González, A. W. H. Chan, R. Vermeylen, M. Shahgholi, T. E. Kleindienst, E. O. Edney, J. H. Offenberg, M. Lewandowski, M. Jaoui, W. Maenhaut, M. Claeys, R. C. Flagan and J. H. Seinfeld, Organosulfate Formation in Biogenic Secondary Organic Aerosol, *The Journal of Physical Chemistry A*, 2008, **112**, 8345-8378.
11. R. J. Huang, J. Cao, Y. Chen, L. Yang, J. Shen, Q. You, K. Wang, C. Lin, W. Xu, B. Gao, Y. Li, Q. Chen, T. Hoffmann, C. D. O'Dowd, M. Bilde and M. Glasius, Organosulfates in atmospheric aerosol: synthesis and quantitative analysis of PM2.5 from Xi'an, northwestern China, *Atmos. Meas. Tech.*, 2018, **11**, 3447-3456.
12. R. Xu, Y. Ge, K. C. Kwong, H. Y. Poon, K. R. Wilson, J. Z. Yu and M. N. Chan, Inorganic Sulfur Species Formed upon Heterogeneous OH Oxidation of Organosulfates: A Case Study of Methyl Sulfate, *ACS Earth and Space Chemistry*, 2020, **4**, 2041-2049.
13. P. R. Bevington, D. K. Robinson, J. M. Blair, A. J. Mallinckrodt and S. McKay, Data Reduction and Error Analysis for the Physical Sciences, *Computers in Physics*, 1993, **7**, 415-416.
14. S. Ellison, M. Roesslein, A. Williams, M. Berglund, W. Haesselbarth, K. Hedegaard, R. Karls, M. Mansson, R. Stephany, A. van der Veen, W. Wegscheider, H. Wiel, R. Wood, P. rong, M. Salit, A. Squirrell, K. Yususda, R. Johnson, J.-K. Lee and D. Galsworthy, *Eurachem/CITAC Guide CG4. Quantifying Measurement Uncertainty in Analytical Measurement*, 2000.
15. P. Eastman, J. Swails, J. D. Chodera, R. T. McGibbon, Y. Zhao, K. A. Beauchamp, L.-P. Wang,

A. C. Simmonett, M. P. Harrigan, C. D. Stern, R. P. Wiewiora, B. R. Brooks and V. S. Pande, OpenMM 7: Rapid development of high performance algorithms for molecular dynamics, *PLOS Computational Biology*, 2017, **13**, e1005659.
16. G. Lamoureux and B. t. Roux, Modeling induced polarization with classical Drude oscillators: Theory and molecular dynamics simulation algorithm, *The Journal of Chemical Physics*, 2003, **119**, 3025-3039.
17. G. Lamoureux, E. Harder, I. V. Vorobyov, B. Roux and A. D. MacKerell, A polarizable model of water for molecular dynamics simulations of biomolecules, *Chemical Physics Letters*, 2006, **418**, 245-249.
18. L. Huang and B. Roux, Automated Force Field Parameterization for Nonpolarizable and Polarizable Atomic Models Based on Ab Initio Target Data, *Journal of Chemical Theory and Computation*, 2013, **9**, 3543-3556.
19. H. Yu, T. W. Whitfield, E. Harder, G. Lamoureux, I. Vorobyov, V. M. Anisimov, A. D. MacKerell and B. Roux, Simulating Monovalent and Divalent Ions in Aqueous Solution Using a Drude Polarizable Force Field, *Journal of Chemical Theory and Computation*, 2010, **6**, 774-786.
20. J. Wang, R. M. Wolf, J. W. Caldwell, P. A. Kollman and D. A. Case, Development and testing of a general amber force field, *Journal of Computational Chemistry*, 2004, **25**, 1157-1174.
21. R. D. Johnson, NIST 101. Computational Chemistry Comparison and Benchmark Database, http://cccbdb.nist.gov.*Journal*, 1999, (accessed June 2020).
22. M. Roeselová, J. Vieceli, L. X. Dang, B. C. Garrett and D. J. Tobias, Hydroxyl Radical at the Air−Water Interface, *Journal of the American Chemical Society*, 2004, **126**, 16308-16309.
23. J. Kästner, Umbrella sampling, *WIREs Computational Molecular Science*, 2011, **1**, 932-942.
24. H. K. Lam, R. Xu, J. Choczynski, J. F. Davies, D. Ham, M. Song, A. Zuend, W. Li, Y. L. S. Tse and M. N. Chan, Effects of liquid–liquid phase separation and relative humidity on the heterogeneous OH oxidation of inorganic–organic aerosols: insights from methylglutaric acid and ammonium sulfate particles, *Atmos. Chem. Phys.*, 2021, **21**, 2053-2066.
25. S. Gopalakrishnan, P. Jungwirth, D. J. Tobias and H. C. Allen, Air−Liquid Interfaces of Aqueous Solutions Containing Ammonium and Sulfate: Spectroscopic and Molecular Dynamics Studies, *The Journal of Physical Chemistry B*, 2005, **109**, 8861-8872.
26. T. D. Kühne, M. Iannuzzi, M. Del Ben, V. V. Rybkin, P. Seewald, F. Stein, T. Laino, R. Z. Khaliullin, O. Schütt, F. Schiffmann, D. Golze, J. Wilhelm, S. Chulkov, M. H. Bani-Hashemian, V. Weber, U. Borštnik, M. Taillefumier, A. S. Jakobovits, A. Lazzaro, H. Pabst, T. Müller, R. Schade, M. Guidon, S. Andermatt, N. Holmberg, G. K. Schenter, A. Hehn, A. Bussy, F. Belleflamme, G. Tabacchi, A. Glöß, M. Lass, I. Bethune, C. J. Mundy, C. Plessl, M. Watkins, J. VandeVondele, M. Krack and J. Hutter, CP2K: An electronic structure and molecular dynamics software package - Quickstep: Efficient and accurate electronic structure calculations, *The Journal of Chemical Physics*, 2020, **152**, 194103.
27. C. Lee, W. Yang and R. G. Parr, Development of the Colle-Salvetti correlation-energy formula into a functional of the electron density, *Physical Review B*, 1988, **37**, 785-789.
28. S. Grimme, J. Antony, S. Ehrlich and H. Krieg, A consistent and accurate ab initio parametrization of density functional dispersion correction (DFT-D) for the 94 elements H-Pu, *The Journal of Chemical Physics*, 2010, **132**, 154104.
29. S. Goedecker, M. Teter and J. Hutter, Separable dual-space Gaussian pseudopotentials, *Physical Review B*, 1996, **54**, 1703-1710.
30. J. D. Weeks, D. Chandler and H. C. Andersen, Role of Repulsive Forces in Determining the Equilibrium Structure of Simple Liquids, *The Journal of Chemical Physics*, 1971, **54**, 5237-5247.
31. R. Xu, H. K. Lam, K. R. Wilson, J. F. Davies, M. Song, W. Li, Y. L. S. Tse and M. N. Chan, Effect of inorganic-to-organic mass ratio on the heterogeneous OH reaction rates of erythritol:

implications for atmospheric chemical stability of 2-methyltetrols, *Atmos. Chem. Phys.*, 2020, **20**, 3879-3893.
32. J. A. Faust and J. P. D. Abbatt, Organic Surfactants Protect Dissolved Aerosol Components against Heterogeneous Oxidation, *The Journal of Physical Chemistry A*, 2019, **123**, 2114-2124.
33. S. L. Clegg, J. H. Seinfeld and P. Brimblecombe, Thermodynamic modelling of aqueous aerosols containing electrolytes and dissolved organic compounds, *Journal of Aerosol Science*, 2001, **32**, 713-738.